Journal of Telecommunication, Electronic and Computer Engineering
ISSN: 2180 – 1843 e-ISSN: 2289-8131 Vol. 18 No. 1 (2026) 1-8
jtec.utem.edu.my
DOI: https://doi.org/10.54554/jtec.2026.18.01.001

Design of a Robust Free-Running Solar Inverter Power Conversion Unit for Instantaneous Backup with Near-Sinusoidal Output

Tanvir Ahmed[1*], Fariha Rahman[1], Ishtiaq Murshed[2], Tanmoy Datta[3], Md.Arman Ali[4]
[1]*Department of Electrical and Electronic Engineering, Jamalpur Science & Technology University, Jamalpur, Bangladesh*
[2]*Department of Chemical Engineering, Bangladesh University of Engineering and Technology, Dhaka, Bangladesh*
[3]*Department of Electrical and Electronic Engineering, Jashore University of Science and Technology, Jashore, Bangladesh*
[4]*Department of Electrical and Electronic Engineering, Southeast University, Tejgaon, Dhaka, Bangladesh*

Article Info
Article history:
Received July 10th, 2025
Revised Mar 6th, 2026
Accepted Mar 26th, 2026
Published Mar 31st, 2026

Index Terms:
DC-AC converter
Efficient solar inverter
Solar UPS
Sine wave inverter
Electronic filter circuit

Abstract
This paper presents a small, scalable, and affordable solar-powered inverter system, designed to provide a continuous power supply in off-grid settings and during grid outages worldwide. The proposed system utilizes lithium-ion batteries charged by solar energy to power a high-efficient and low power dissipation inverter constructed using durable power transistors, a step-up transformer, and a custom-designed filter circuit. The inverter generates a near-sinusoidal AC output capable of supporting a wide range of loads, thereby reducing dependency on fuel-generated grid electricity, particularly in underserved regions. The system emphasizes cost-free energy storage and reducing energy losses within components. It maintains a stable near-sinusoidal voltage under practical load conditions. The modular design integrates energy conversion, storage, and AC power delivery into a unified system. With a Total Harmonic Distortion (THD) of only 2.17%, the inverter delivers high-quality voltage output with a near-sinusoidal waveshape at lower complexity compared to conventional systems. The system is suitable for mobile applications, emergency supply of power during outages, disaster relief, and rural electrification. The proposed solution demonstrates the accessibility and effectiveness of solar technology in practical, real-world applications.

*Corresponding Author: tanvir.s21111214@jstu.ac.bd

I. INTRODUCTION

The increasing number of power outages and interruptions, particularly in remote and infrastructure-limited areas, has created a strong need for compact, energy-efficient, fuel-independent, easily serviceable, and cost-effective backup power solutions. Traditional inverters often suffer from several limitations: they are bulky, complex to repair or modify, dissipate excessive energy within circuitry components, operate inefficiently under variable loads, are expensive, and produce high harmonic distortion. These issues often lead to unstable performance when powering sensitive electronic equipment [1], [2].

To address these challenges, we developed a compact, modular, low-energy-dissipation solar inverter system. The proposed system integrates solar charging, lithium-ion battery storage, and a high- efficiency DC-to-AC conversion stage by a custom-designed inverter circuit combined with a filtering stage [3].

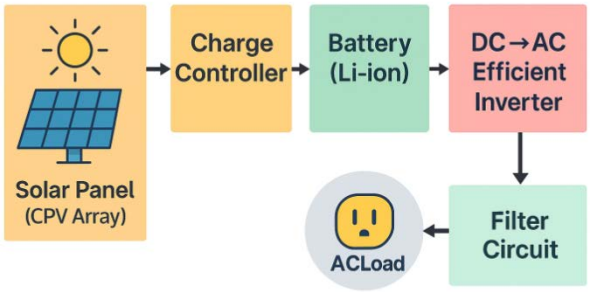

Figure 1. Core block layout showing solar charging, battery storage, inverter switching, and filter stage for AC output.

Figure 1 illustrates the overall system architecture, including the solar input, storage unit, inverter switching section, and passive filtering stage. This system operates fully autonomously and delivers a continuous, near-sine-wave AC output, achieved through a carefully engineered advanced passive filter circuit. This filter effectively minimizes harmonic distortion without relying on digital processing or complex control systems, thereby producing a stable near-sinusoidal output suitable for sensitive electronic device [4].

All stages of the proposed system collectively ensure stable and highly efficient power delivery. The all-in-one architecture integrates solar harvesting, energy storage, and AC power generation into a streamlined plug-and-play unit with zero running cost. This integrated design makes the proposed system ideal for off-grid, mobile, or emergency applications, particularly in underserved and infrastructure-limited communities, which represent a significant portion of the global population. The circuit emphasizes simplicity through analog design with a reduced component count, allowing convenient simulation in LTspice or other circuit simulation software and facilitating a smooth transition to real hardware implementation. This work therefore offers a practical, durable, and scalable solution to meet essential energy needs in resource-constrained and marginalized environments.

Furthermore, its portability, minimal maintenance requirements, and autonomous operation make the system especially suitable for rural electrification, disaster relief, and sustainable energy applications. The output voltage of the circuit exhibits a Total Harmonic Distortion (THD) of 2.17%, indicating a low level of harmonic content and good voltage quality [5]. Its cost efficiency, fuel independence, fuel independence, affordable circuitry, and low THD(%) make the system both novel and practical. Future versions may further improve waveform purity and overall system integration through optimized filter designs or hybrid analog-digital control methods, if required [6].

II. RESEARCH METHODOLOGY

A. Transformer Design for Inverter Application

This study included the design and fabrication of a real-world 220V to 12V, 7A step-down transformer, suitable for use in UPS and inverter systems for power conversion applications. The transformer was specifically designed for bidirectional operation to enable multi-functional applicability. In grid-connected mode, it stepped down 220V AC to 12V DC for battery charging or load support. In inverter mode, the transformer operated in reverse, stepping up 12V from a battery to produce 220V AC using switching topologies such as push-pull or full-bridge inverters. Table 1 shows the transformer design parameters, and Figure 2 ilustrates the simulated circuit diagram [7].

The transformer was designed for 50 Hz AC operation with a target power capacity of approximately 84 watts. A laminated EI-type silicon steel core was selected due to its low hysteresis loss, good thermal stability, and wide commercial availability [8]. The primary winding (220V) was wound with thinner enamel-coated copper wire, while the secondary winding (12V) utilized thicker wire to handle higher currents with minimal copper losses. Transformer design and simulation were conducted to verify voltage conversion performance and ensure proper electrical isolation between circuits. These processes also supported need-based customization of material and structural parameters, enabling efficient power transfer and minimizing potential losses prior to practical implementation.

Table 1
Transformer design parameters

Parameter	Value	Notes
Primary Voltage (AC RMS)	220V	Real-life input
Primary Inductance (L1)	10 mH	Simulated in LTspice
Secondary Voltage (AC RMS)	12V (center tap)	6V–0–6V
Secondary Inductance (Ls1, Ls2)	8 µH each	Based on turns ratio
Turns Ratio	~18.3:1	Primary : Secondary
Max Load Current	7A	On secondary
Load Resistance	2 Ω	For 12V @ 7A
Frequency	50 Hz	Power line frequency
Coupling Factor (K)	0.98–0.995	Realistic iron-core transformer
Transformer Power Rating	≈ 100 VA	Realistic based on 12V, 7A

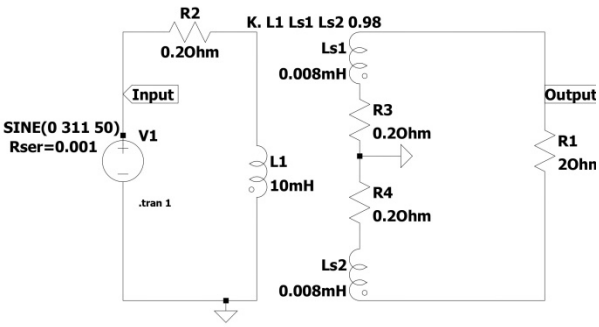

Figure 2. Transformer Circuit Diagram

The required number of turns was calculated using the standard EMF equation shown in (1).

$$N = \frac{V}{4.44 \times f \times B_{max} \times A_c} \quad (1)$$

Where V is the voltage in volts, f is the frequency in Hz (typically 50 Hz), B_{max} is the peak flux density (usually 1.2 Tesla), and A_c is the core's cross-sectional area in square meters.

For this specific design, the 12V winding was energized through a battery-driven MOSFET switching inverter circuit

along with other components such as resistors. Alternating polarity pulses delivered to the transformer induced a stepped-up AC voltage at the 220V winding. Proper waveform symmetry and duty cycle balance were maintained to prevent core saturation and minimize waveform distortion. The bidirectional behavior of the transformer also supported more complex hybrid inverter designs. This process involved both charging and discharging operations, which were efficiently handled by the same magnetic core of the transformer. The transformer was hand-wound, insulated, and tested under resistive loads in both forward and reverse configurations. Various practical measurements confirmed stable voltage regulation, minimal temperature rise, and reliable startup, even under inverter-driven square-wave conditions. No acoustic noise or overheating issues were observed during extended laboratory operation.

This transformer design offers notable advantages over typical off-the-shelf models. Its dual-mode optimization enables both charging and power delivery through a single magnetic structure, significantly reducing system cost and complexity. Its real-world performance and practical behavior validate its suitability for use in cost effective, high-efficiency inverter systems, especially in underserved regions or UPS-based power applications.

B. Filter Design for Square-to-Sine Wave Conversion

To transform a ±110 V square-wave input into a near-sinusoidal output with low total harmonic distortion (THD), a robust and durable passive filter was developed during this research. This filter comprises a multi-stage R_1–L_1–R_2–C_1–C_2–C_3 topology, augmented by a bidirectional MOV (Metal Oxide Varistor) voltage clamp for spike suppression and enhanced durability [9]. Table 2 presents the filter circuit design parameters, and Figure 3 illustrates the filter circuit diagram.

A low-pass/band-pass filter configuration was employed, allowing the fundamental frequency (50 Hz) to pass while effectively attenuating higher-order harmonics. The LC cutoff frequency was calculated using the standard formula shown in (2).

$$f_c = \frac{1}{2\pi\sqrt{LC}} \quad (2)$$

The key design objective was harmonic suppression. The values L_1 = 1.5 H and $C_1 = C_2 = C_3$ = 4.7 µF were selected, resulting in a bandwidth that excluded frequencies above 150 Hz .

A series damping resistor R_2 = 30 Ω was incorporated within the filter to flatten the frequency response and reduce resonance peaks commonly associated with LC filters. This damping improved real-world stability and minimized signal reflections, which are critical in non-ideal and practical environments.

To protect the circuit against voltage spikes caused by load transients or switching noise, bidirectional MOVs such as the EPCOS B72220S301K101 were employed. The device effectively clamped voltage surges and maintained safe voltage levels. Compared to traditional Zener-based voltage control methods, MOV shows superior performance in practical applications, enhancing overall stability and loud compatibility.

Testing on a laboratory prototype powered by a 220 V square-wave inverter source confirmed the predicted performance of the developed filter circuit. The output waveform closely resembled a pure sine wave, and the measured THD under no-load conditions remained very low, only 2.17%.

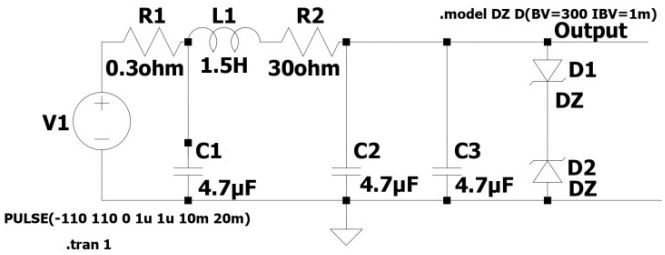

Figure 3. Filter Circuit Diagram

Table 2
Filter Circuit Design Parameters

Component	Value	Description
R1	0.3 Ω	Input series resistor
L1	1.5 H	Series inductor for filtering
R2	30 Ω	Damping resistor after inductor
C1	4.7 µF	Input-side filter capacitor
C2	4.7 µF	Intermediate filter capacitor
C3	4.7 µF	Final filter capacitor before output
Metal Oxide Varistor- MOV	275V AC	300 V Zener diode used to simulate MOV clamping.
V1	PULSE(-110V to +110V)	Input voltage source with rise/fall time 1µs, width 10ms, period 20ms

Our solution provided a high-order passive filter with integrated damping and surge protection system, which were crucial and highly desirable in power electronics applications. While active filter required operational amplifiers and complex feedback control, the proposed approach was inherently simpler to repair, more compact and highly suitable for inverter-based power systems, particularly in decentralized setups.

The entire circuit was designed for long operational life,

very low power loss, and strong mechanical and electrical robustness. It operated more reliably than many traditional filter designs. The output waveform closely approximated a pure sine wave and the system was able to operate for thousands of cycles without significant performance degradation. It was therefore suitable for low-cost and long-lasting inverter applications. The inverter converted low-voltage DC from a solar-charged battery into stable AC power for residential and small industrial loads. Figure 4 shows the main circuit. At the input stage, a 275 V RMS Metal Oxide Varistor (MOV) was connected to protect the circuit from sudden voltage surges when the AC load was connected. Three 4.7 µF metalized polypropylene BMPP capacitors, rated at 450 V, were connected in a π-filter arrangement. These capacitors helped reduce harmonic distortion and smoothed the output AC waveform. A 1.5 H inductor (L2), a 10 mH inductor (L1), and resistors R3 and R4 were also used. Together they formed an LCL filter. This filter, which reduced switching noise and improved the output waveform [10].

The inverter used a center-tapped step-up transformer, with the primary winding operating in a push-pull mode. Two D13007 high-voltage, fast-switching power transistors were used for switching, each connected with a 470 Ω resistor (R1 and R2). Auxiliary coils Ls1 and Ls2 provided inductive feedback for switching control. The transistors switched one alternately, energizing each half of the transformer primary in turn. This operation produced AC voltage at the secondary side. The output then passed through the filter before being supplied to the AC load. A 12 V battery supplied the inverter, while a solar charge controller regulated battery charging according to system parameters. This ensured safe and efficient solar energy harvesting and stable inverter operation.

C. Inverter Circuit Development

The inverter circuit converted 12V DC from a solar battery into AC power for household use. Figure 4 shows the circuit diagram. At the input, a 275V RMS Metal Oxide Varistor (MOV) was connected to absorb voltage spikes during the first few milliseconds when the AC side was connected, thereby protecting the other components in the circuit.

For harmonic and noise filtering, three 4.7 µF high-voltage BMPP capacitors (C1, C2, C3), a 1.5H inductor (L2), and two resistors (R3 = 0.3Ω and R4 = 5Ω) were used. These components formed an LC filter network. The filter smoothed the voltage waveform and reduced transient noise before the signal entered the inverter stage. In the practical setup, the 30Ω resistor was replaced with a 5Ω resistor to reduce power loss. While a 30Ω resistor provided better damping of high-frequency harmonics, it resulted in higher I^2R losses, thereby reducing overall system efficiency. The 5Ω resistor reduced power loss and heat generation. Although the output waveform became slightly less sinusoidal, the reduction in losses was considered more important for a low-power battery system. This setup was suitable for resistive and non-critical loads. Figure 4 shows the full circuit diagram, and Figure 5 shows the built inverter prototype with the sine wave filter [11].

The inverter used a push-pull circuit with two D13007 transistors. Each transistor was connected with a 470Ω resistor (R1 and R2). Feedback was provided by transformer coils Ls1 and Ls2. The transistors switched alternately, generating AC at the output. A center-tapped transformer raised 12V DC to the required AC level and provided isolation between input and output. The developed hardware prototype is shown in Figure 5.

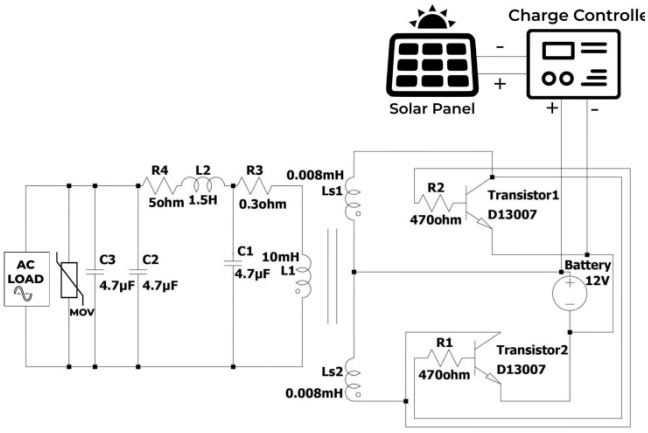

Figure 4. Complete Circuit Diagram

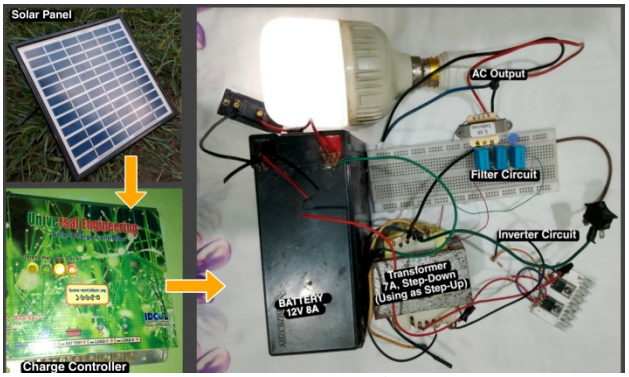

Figure 5. Hardware Implementation of the Proposed System

D. Battery Placement

The system achieved optimal performance using lithium iron phosphate ($LiFePO_4$) batteries. These batteries were selected due to their high safety, long lifespan and thermal stability. $LiFePO_4$ materials exhibited relatively low electrical conductivity, therefore, conductive coatings were applied during the battery manufacturing process to enhance current flow. Carbon-based materials, metals, and metal oxides were used to improve electron and ion transport. Proper material mixing and treatment improved overall battery performance [12].

E. Solar Panel and Charge Controller

Monocrystalline solar panels were selected for this system due to their efficiency and ability to generate substantial power from a limited surface area. A charge controller was installed between the solar panel and the battery to regulate charging process. It controlled charging and protected the system from overcharging, deep discharge, and short circuits. Additionally, it managed power flow from the solar panel to the battery, ensuring stable and efficient operation [13].

III. RESULTS AND DISCUSSION

A. Transformer Operation and Performance

The transformer was tested in time-domain simulation for low-voltage inverter applications. The primary winding had and induction of ten millihenry. The secondary side consisted of two small coupled windings. The coupling coefficient was close to unity, indicating strong magnetic coupling. A sinusoidal input was applied to the primary at standard mains frequency. The primary waveform remained smooth and sinusoidal. The secondary output produced a clean sine wave with lower voltage, consistent with the expected step-down operation. Minor deviations from the ideal value were attributed to winding resistance and leakage inductance. The waveform shape remained stable and suitable for the inverter output stage. The simulation results closely matched the hardware behavior and validated proper transformer operation in practice. Figure 6 shows the simulated primary and secondary simulated waveforms [14].

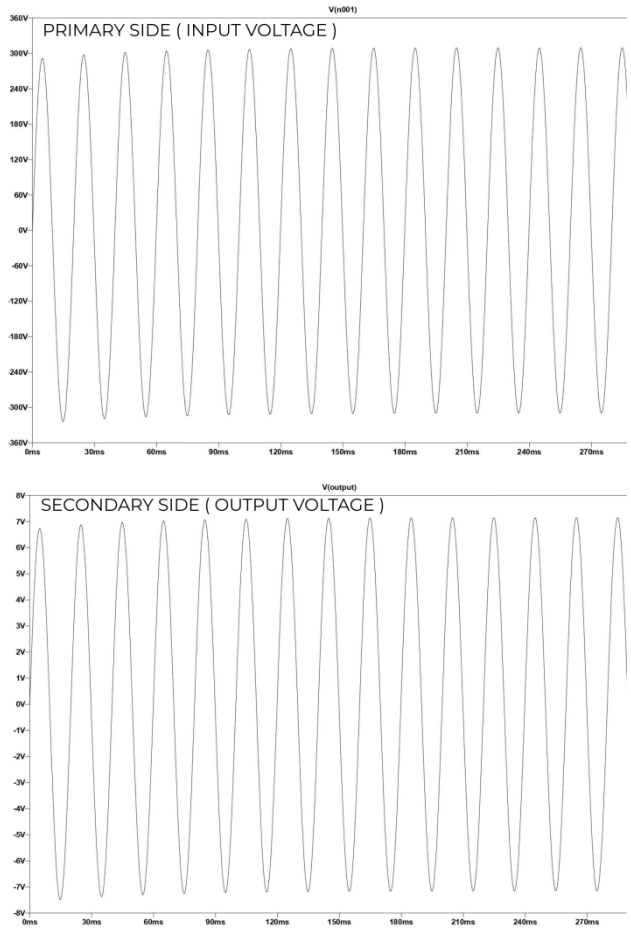

Figure 6. Simulated Primary Input and Secondary Output Waveforms of the Transformer.

B. Sine wave filter performance and THD calculation

The filter circuit was tested using a square-wave input generated from the developed inverter topology. The objective was to transform the stepped waveform into a near sine wave with very low THD. The circuit utilized a π-filter made of inductors and capacitors. A metal oxide varistor was included to absorb sudden voltage spikes. Simulation results showed that the output waveform became progressively smoother over time. Harmonics components were significantly reduced, and the waveform approached a sinusoidal shape The filter effectively reduced sharp edges and high-frequency noise. The design employed simple passive components, making it easy to build and repair. It was adaptable to various inverter types, especially solar-based systems. The compact structure allowed integration into small inverter cases.

Figure 7 shows the filter performance waveform. The filter supported continuous load operation in solar inverter systems such UPS and off-grid applications. The MOV provided protection during sudden load changes [15]. Overall, the design converted a square-wave output into a smooth AC waveform with reduced distortion and noise.

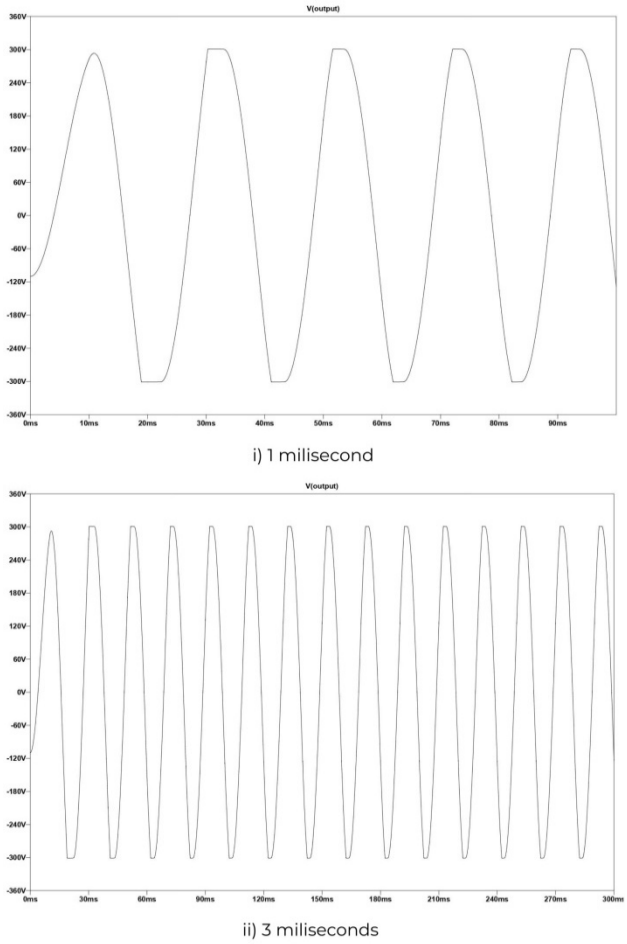

Figure 7. Filter Performance Curve Showing Sinusoidal Output Shaping.

C. Full System Performance Analysis

The full inverter system was tested with the LC π-filter connected at the output. A square switching signal was applied at the inverter stage. The filter shaped the output into a near-sinusoidal waveform. Both simulation and oscilloscope results showed reduced harmonic content. The inductors and capacitors acted as a multi-stage low-pass filter, reducing high-frequency components generated by the switching process.

A metal oxide varistor was placed at the output for surge protection. It absorbed sudden voltage spikes without affecting normal operation. The filter used only passive components, ensuring a simple structure. Power losses were low, and heat generation was limited. The system operated under different load conditions without instability. Figure 8 shows the measured output waveform during testing. The

results confirmed proper waveform shape and steady operation. The design focused on low cost, ease of maintenance, and practical application in small and off-grid power systems.

THD Calculation: Total Harmonic Distortion (THD) was defined as the ratio of the RMS value of all harmonic components (excluding the fundamental) to the RMS value of the fundamental component [16].

$$\text{THD}(\%) = \frac{\sqrt{V_2^2 + V_3^2 + V_4^2 + \cdots + V_n^2}}{V_1} \quad (3)$$

where V_1= RMS voltage of the fundamental component, and V_2, V_3, V_4= RMS voltages of harmonic components.

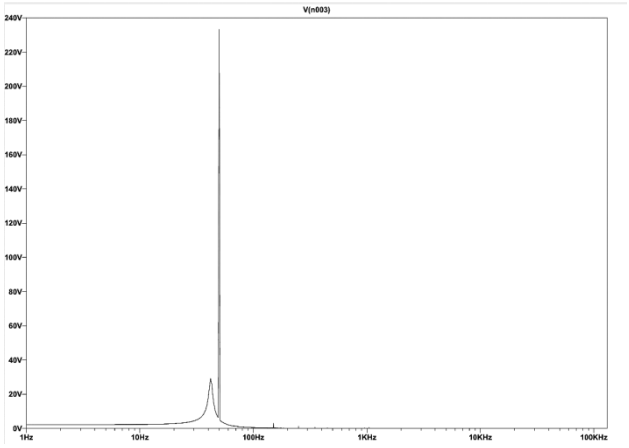

Figure 8. Linear FFT of V(out) – Voltage(X-axis) vs Frequency(Y-axis)

The FFT (Fast Fourier Transform) spectrum shown in Figure 8 illustrated the frequency components of the output voltage. The tallest peak represented the fundamental component, while the smaller peaks indicated harmonic components. FFT analysis was used to evaluate power quality and quantify distortion through THD [17]. The analysis demonstrated how effectively the filter reduced unwanted harmonics in the inverter output [18]. Data used for THD calculation are presented in Table 3.

Table 3
Harmonic order, frequency and RMS voltage calculation

Harmonic Order (n)	Frequency(Hz)	RMS Voltage (V)
1 (Fundamental)	50	230
3rd	150	3.30
5th	250	2.30
7th	350	1.80
9th	450	1.40
11th	550	1.10
13th	650	1.421

Harmonic RMS Calculation:

$$V_{\text{harmonics}} = \sqrt{(3.30)^2+(2.30)^2+(1.80)^2+(1.40)^2+(1.10)^2+(1.421)^2}$$

$$= \sqrt{24.910}$$

=4.991V

Based on Table 3, the fundamental voltage $V_1 \approx 230$V; and the total harmonic RMS (combined small components) ≈ 5 V

$$\text{THD}(\%) = \frac{V_{\text{harmonics}}}{V_1} \times 100\%$$

$$= 2.17\%$$

Oscilloscope Validation:

The complete inverter circuit was tested multiple times in the electronics circuit laboratory under various arrangements, showed in Figure 9. The output voltage waveform closely matched the simulated waveform. Other performance parameters were also satisfactory for operating real-life loads.

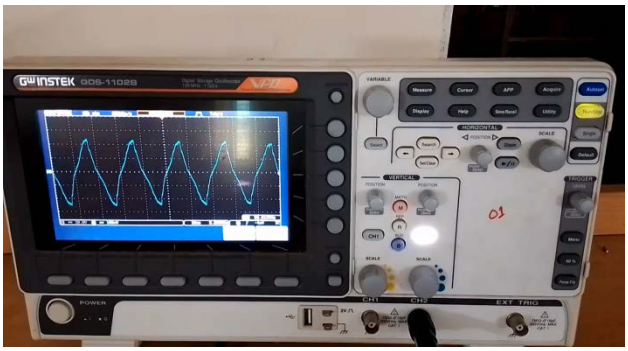

Figure 9. Output Oscilloscope Waveform of the Inverter Circuit

Frequency Regulation and Practical Observation: The output frequency was not exactly 50 Hz during testing due to the transistor-based switching oscillator. Variations in components and load conditions also contributed to frequency deviations. LED and bulb loads operated normally, while motor-driven and clock-based loads did not perform optimally. Motors rotated at non-standard speeds and the lifespan of some devices could be affected. The integration of a more stable oscillator or PWM control could improve frequency regulation [19]. Table 4 shows the performance of the inverter when different loads were connected.

Table 4
Scalability Performance of the Solar Inverter with Different Load Conditions

Load (W)	Output Voltage(V)	Output Current (A)	Efficiency (%)
10 W	221 V	0.05 A	85 %
20 W	218 V	0.09 A	84 %
40 W	214 V	0.18 A	82 %
60 W	210 V	0.27 A	80 %

The testing was conducted using various LED and tungsten bulbs as practical loads. Measurements were taken using multimeters and wattmeter. As the load increased, the output voltage slightly decreased. Efficiency was calculated using the relation Efficiency (%) = (Output Power / Input Power) × 100. Efficiency decreased slightly at higher loads due to increased power losses as heat within the components [20]. The Load vs Efficiency graph in Figure 10 shows how the inverter efficiency changes with increasing load [21].

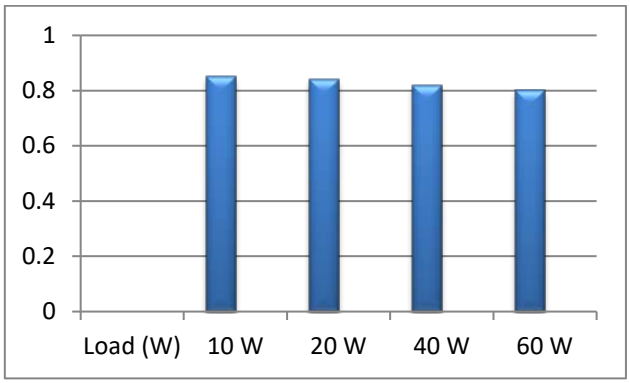

Figure 10. Load (X-axis) vs Efficiency (Y-axis) Graph.

The results indicated that efficiency decreased at higher loads due to increased internal power losses in the transformer and switching components [22].

IV. CONCLUSION

The analysis and testing confirmed that the proposed inverter operated as a practical solar-powered AC system. It converted solar-charged DC into usable AC output using a simple square wave stage combined with a passive filter. The measured Total Harmonic Distortion (THD) was 2.17%, calculated from linear FFT analysis. The results indicated that the output waveform closely approximated a sine wave and suitable for common electrical loads. The circuit did not rely on complex control ICs or digital modulation; instead, it utilized simple and readily available components. A metal oxide varistor protected the output from voltage surges, while the filter smoothed the waveform under stable input conditions. The system successfully operated loads such as bulbs and fans, even under open-loop conditions. The inverter was powered by a solar-charged 12V source and did not depend on complex digital control, making it well-suited for off-grid and rural applications. The design was easy to repair and could be expanded if required.

Overall, the system was low-cost and economically practical. Component costs were minimal, and maintenance requirements were simple. The results demonstrated that carefully designed passive filtering could produce clean AC power without the need for expensive circuitry. The system proves that a basic square wave inverter was capable of delivering a smooth sine-wave-like output with 2.17% THD and reliable real-world performance.

CONFLICT OF INTEREST

The authors declare that there is no conflict of interest regarding the publication of this research work.

AUTHOR CONTRIBUTION

Tanvir Ahmed led the project from concept to completion, including circuit design, simulation, hardware implementation, testing, and manuscript preparation. Fariha Rahman contributed significantly to the simulation work and assisted in analyzing the performance results. Ishtiaq Murshed provided focused input on the battery integration segment of the methodology and assisted with technical validations. Tanmoy Datta and Md. Arman Ali supported the study through background literature review and analysis of existing inverter hardware. The work was carried out under the overall guidance and coordination of Tanvir Ahmed. All authors contributed to discussions, reviewed the manuscript, and approved its final version.

REFERENCES

[1] S. Adak and H. Cangi, “Elimination of harmonic components in solar system with L and LC passive filters,” International Journal of Energy and Smart Grid, vol. 6, no. 1-2, pp. 14-27, 2021.

[2] K. M. Alawasa, “Measurement-based analysis of power quality and harmonic distortion characteristics for electric vehicle AC charging modes,” World Electric Vehicle Journal, vol. 17, no. 2, p. 108, 2026.

[3] X. Kong, P. Zhang, L. Ma, Z. Zhu, X. Liu and K. Y. Lee, “Finite-control-set economic model predictive control for a DC/AC inverter,” Control Engineering Practice, vol. 163, p. 106385, 2025.

[4] F. S. Aamara, P. K. Balachandran, Y. Yusof and M. A. Mohd Radzi, “Hybrid passive damping filter of single-phase grid-tied PV-micro inverter,” International Journal of Electrical & Computer Engineering, vol. 15, no. 4, 2025.

[5] P. Thayumanavan, D. Kaliyaperumal, U. Subramaniam, M. S. Bhaskar, S. Padmanaban, Z. Leonowicz and M. Mitolo, “Combined harmonic reduction and DC voltage regulation of a single DC source five-level multilevel inverter for wind electric system,” Electronics, vol. 9, no. 6, p. 979, 2020.

[6] A. I. M. Ali, S. M. Saeed, A. Hassan, A. Belahcen, M. Aly and J. Rodríguez, “Single-stage grid-connected inverter with selective harmonic elimination for solar PV applications,” in Proc. 26th Int. Middle East Power Systems Conf. (MEPCON), pp. 1-6, 2025.

[7] R. Badr, F. Rerhrhaye, L. Ilyas, E. A. Akkary Ahmed, N. Sefiani, N. Mrabet and C. El Martaoui, “Proposal of an interleaved boost converter controlled by a nonlinear MPPT ADRC as the boost stage of a solar inverter connected to the hospital electrical network,” Cleaner Energy Systems, p. 100222, 2025.

[8] A. A. Desai and S. Mikkili, “Improved transformer-less grid-connected PV inverter with CCMV for enhanced efficiency,” CPSS Transactions on Power Electronics and Applications, vol. 10, no. 4, pp. 351-359, 2025.

[9] C. Seng, J. J. Seo, M. H. Min and H. Cha, “LCL filter design for medium power grid-connected inverter considering THD constraint and control stability,” Journal of Electrical Engineering & Technology, 2026.

[10] D. Khan, M. H. Qais, H. Hasanien, S. Alghuwainem, I. Sami and P. Hu, “Enhanced stability of grid-connected inverter using adaptive filtering damping of capacitive current feedback of LCL filter,” Ain Shams Engineering Journal, vol. 16, no. 8, p. 103465, 2025.

[11] M. Alshammari and M. Duffy, “Review of single-phase bidirectional inverter topologies for renewable energy systems with DC distribution,” Energies, vol. 15, no. 18, p. 6836, 2022.

[12] K. Bano and G. Abbas, “Exploring the material feasibility of a LiFePO4-based energy storage system,” Energies, vol. 18, no. 15, p. 4102, 2025.

[13] R. P. David, I. Faisal, V. B. Alamsyah and P. Narputro, “Utilization of solar panels in various applications: A systematic literature review,” Engineering Proceedings, vol. 107, no. 1, p. 33, 2025.

[14] M. Biswas, S. P. Biswas, M. R. Islam, M. A. Rahman, K. M. Muttaqi and S. M. Muyeen, “A new transformer-less single-phase photovoltaic inverter to improve the performance of grid-connected solar photovoltaic systems,” Energies, vol. 15, no. 22, p. 8398, 2022.

[15] Y. Men, X. Lu, Z. Zhang and R. Thiagarajan, “Metal oxide varistor (MOV) lifetime estimation with impulse-based testing in PV inverter systems,” in Proc. IEEE Int. Symp. Power Electronics for Distributed Generation Systems (PEDG), pp. 1-4, 2022.

[16] K. Bano, G. Abbas, M. Hatatah, E. Touti, A. Emara and P. Mercorelli, “Phase shift APOD and POD control technique in multi-level inverters to mitigate total harmonic distortion,” Mathematics, vol. 12, no. 5, p. 656, 2024.

[17] M. Kamal, A. Bostani, J. L. Webber, A. Mehbodniya, R. Mishra and M. Arumugam, “Total harmonic distortion reduction based energy harvesting using grid-based three phase system and integral-derivative,” Computers and Electrical Engineering, vol. 109, p. 108744, 2023.

[18] D. F. Niste, S. G. Pavel, R. A. Tîrnovan, C. G. Martineac and H. G. Beleiu, “Analyzing the impact of harmonics in industrial networks using FFT in Matlab,” in Proc. Int. Conf. Energy and Environment (CIEM), pp. 1-6, 2025.

[19] D. Al Kez, A. M. Foley, F. Ahmed and D. J. Morrow, “Overview of frequency control techniques in power systems with high inverter-based resources: Challenges and mitigation measures,” IET Smart Grid, vol. 6, no. 5, pp. 447-469, 2023.

[20] A. Shameli, M. Maghsoudi and H. Farzanehfard, “Bridgeless cuk PFC converter with soft switching in full input voltage and load range,” IEEE Transactions on Industrial Electronics, vol. 71, no. 7, pp. 6938-6945, 2023.

[21] M. F. Kibria, A. Elsanabary, K. S. Tey, M. Mubin and S. Mekhilef, “A comparative review on single phase transformerless inverter topologies for grid-connected photovoltaic systems,” Energies, vol. 16, no. 3, p. 1363, 2023.

[22] F. Spertino, A. Ciocia, A. Mazza, M. Nobile, A. Russo and G. Chicco, “Voltage control in low voltage grids with independent operation of on-load tap changer and distributed photovoltaic inverters,” Electric Power Systems Research, vol. 211, p. 108187, 2022.